12th International Conference on Topics in Astroparticle and Underground Physics (TAUP 2011) IOP Publishing
Journal of Physics: Conference Series **375** (2012) 042049 doi:10.1088/1742-6596/375/4/042049

Final results from SNO

N Tolich for the SNO collaboration

Center for Experimental Nuclear Physics and Astrophysics, and Department of Physics, University of Washington, Seattle, WA 98195, USA

E-mail: ntolich@u.washington.edu

Abstract. We report results from a combined analysis of solar neutrino data from all phases of the Sudbury Neutrino Observatory. By exploiting particle identification information obtained from the proportional counters installed during the third phase, this analysis improved background rejection in that phase of the experiment. The combined analysis resulted in a total flux of active neutrino flavors from ^{8}B decays in the Sun of $(5.25 \pm 0.16(\text{stat.})^{+0.11}_{-0.13}(\text{syst.})) \times 10^6\,\text{cm}^{-2}\text{s}^{-1}$. A three-flavor neutrino oscillation analysis combining this result with results of all other solar neutrino experiments and the KamLAND experiment yielded $\Delta m^2_{21} = (7.41^{+0.21}_{-0.19}) \times 10^{-5}\,\text{eV}^2$, $\tan^2\theta_{12} = 0.446^{+0.030}_{-0.029}$, and $\sin^2\theta_{13} = (2.5^{+1.8}_{-1.5}) \times 10^{-2}$. This implied an upper bound of $\sin^2\theta_{13} < 0.053$ at the 95% confidence level (C.L.).

1. Introduction

The Sudbury Neutrino Observatory (SNO) was designed to measure the flux of neutrinos produced by ^{8}B decays in the Sun, so-called ^{8}B neutrinos, and to study neutrino oscillations, as proposed by Herb Chen [1]. As a result of measurements with the SNO detector and other experiments, it is now well-established that neutrinos are massive and that the weak eigenstates (ν_e, ν_μ, ν_τ) are mixtures of the mass eigenstates (ν_1, ν_2, ν_3). The probability of detecting a neutrino in the same weak eigenstate in which it was created depends on the energy and propagation distance of the neutrino, the effects of matter [2, 3], the neutrino mixing angles (θ_{12}, θ_{23}, θ_{13}), a phase (δ) that can lead to charge-parity violation, and the differences between the squares of the neutrino mass eigenvalues (Δm^2_{21}, Δm^2_{32}, Δm^2_{31}) [4, 5].

The SNO detector observed ^{8}B neutrinos via three different reactions. By measuring the rate of neutral current (NC) reactions, $\nu_x + d \rightarrow p + n + \nu_x$, which is equally sensitive to all three active neutrino flavors, the SNO experiment determined the total ^{8}B neutrino flux, Φ_{B}, independently of any specific active neutrino flavor oscillation hypothesis [1]. The predicted flux from solar model calculations [6] is $(5.88 \pm 0.65) \times 10^6\,\text{cm}^{-2}\text{s}^{-1}$, BPS09(GS), or $(4.85 \pm 0.58) \times 10^6\,\text{cm}^{-2}\text{s}^{-1}$, BPS09(AGSS09), using a recent measurement of the heavy-element abundance at the Sun's surface. Previous analyses of SNO data [7, 8] measured Φ_{B} more precisely than the solar model predictions. A more precise measurement of Φ_{B} would better constrain these solar models, but may not necessarily determine which metallicity is correct due to the large uncertainties at present on both predictions.

By measuring the rate of charged current (CC) reactions, $\nu_e + d \rightarrow p + p + e^-$, which is only sensitive to ν_es, and comparing this to the NC reaction rate, it was possible to determine the neutrino survival probability as a function of energy. This can then constrain the neutrino oscillation parameters independently of any specific prediction of Φ_{B}.

The SNO experiment also measured the rate of elastic scattering (ES) reactions, $\nu_x + e^- \rightarrow \nu_x + e^-$, which is sensitive to all neutrino flavors, but the cross-section for ν_es is approximately six times larger than that for the other flavors.

2. The SNO Detector

The SNO detector [9] consisted of an inner spherical volume containing 10^6 kg of 99.92% isotopically pure heavy water (^2H_2O, hereafter referred to as D_2O) within a 12 m diameter transparent acrylic vessel (AV). Over 7×10^6 kg of H_2O between the rock and the AV shielded the D_2O from external radioactive backgrounds. An array of 9456 inward-facing 20 cm Hamamatsu R1408 photomultiplier tubes (PMTs), installed on an 17.8 m diameter stainless steel geodesic structure, detected Cherenkov radiation produced in both the D_2O and H_2O.

The recoil electrons from both the ES and CC reactions were detected directly through their production of Cherenkov light. The total amount of light detected by the PMT array was correlated with the energy of the interacting neutrino.

The SNO detector operated in three phases distinguished by how the neutrons from the NC interactions were detected. In Phase I, the detected neutrons captured on deuterons in the D_2O releasing a single 6.25 MeV γ-ray, and the Cherenkov light of secondary Compton electrons or e^+e^- pairs was detected. In Phase II, 2×10^3 kg of NaCl were added to the D_2O, and the neutrons captured predominantly on ^{35}Cl nuclei, which have a much larger neutron capture cross-section than deuterium nuclei, resulting in a higher neutron detection efficiency. Capture on chlorine also released more energy (8.6 MeV) and yielded multiple γ-rays, which aided in identifying neutron events. In Phase III, an array of proportional counters (the Neutral Current Detection, or NCD, array) was deployed in the D_2O [10]. Thirty-six of the proportional counters were filled with ^{3}He, and neutrons were detected via the reaction $^3\mathrm{He} + n \rightarrow {}^3\mathrm{H} + p$. Four proportional counters were filled with ^{4}He that were insensitive to the neutron signals and were used to study backgrounds. Energetic charged particles within the proportional counters produced ionization electrons, and the induced voltage caused by these electrons was recorded as a function of time, referred to as a waveform.

3. Analysis

In this article we present an analysis that combines data from all three phases of the SNO experiment, with the details given in Ref. [11]. The combination accounts for any correlations in the systematic uncertainties between phases. The data were split into day and night sets in order to search for matter effects as the neutrinos propagated through the Earth.

The general form of the analysis was a fit to Monte Carlo-derived probability density functions (PDFs) for each of the possible signal and background types. For Phases I and II the following four variables calculated from the PMT array were used to construct 4-dimensional PDFs: the effective electron kinetic energy, T_{eff}, reconstructed under the hypothesis that the light was caused by a single electron; the cube of the radial position, r, divided by 600 cm, $\rho = (r^{[\mathrm{cm}]}/_{600})^3$; the isotropy of the detected light, β_{14}; and the angle of the reconstructed electron propagation relative to the direction of the Sun, $\cos\theta_\odot$. For Phase III the reduced number of NC events observed with the PMT array made the β_{14} event variable unnecessary, so the PDFs were 3-dimensional in T_{eff}, ρ, and $\cos\theta_\odot$.

For data from the NCD array in Phase III, the number of neutron events was determined from a likelihood fit to a histogram of the energy deposited in the gas of a proportional counter, E_{NCD}, with 50 bins uniformly spaced between 0.4 and 0.9 MeV. The PDF of E_{NCD} for neutron events was obtained from calibration data, and for alpha events it was approximated by a polynomial. A particle identification cut was developed based on the correlated waveform. The waveforms of neutron events could be significantly broader than those from alpha events, depending on the orientation of the proton-triton trajectory. In an attempt to reduce the number of alpha events,

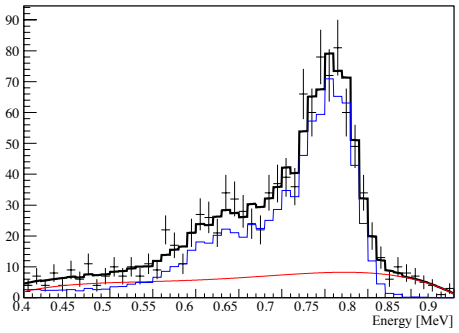

Figure 1. The fitted $E_{\rm NCD}$ spectrum after the particle identification cut. The thick black line is the best fit. The blue and red lines are the best fitted neutron and alpha spectra, respectively.

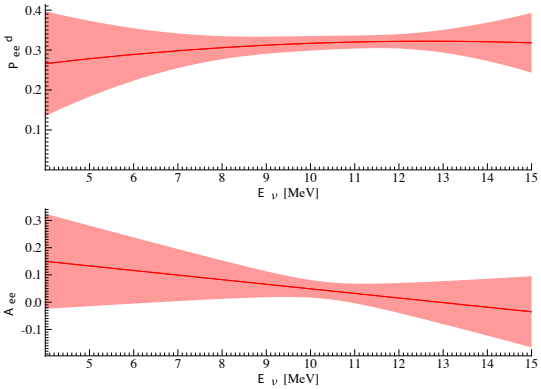

Figure 2. RMS spread in $P^{\rm d}_{ee}(E_\nu)$ and $A_{ee}(E_\nu)$, taking into account the parameter uncertainties and correlations. The solid lines are the best fits.

and therefore the uncertainties associated with them, we developed a particle identification cut that removed almost all the events on the strings filled with ^{4}He, i.e. alpha events, while maintaining $(74.78 \pm 0.68)\%$ of the ^{24}Na calibration events, i.e. neutron events.

The Monte Carlo simulation was verified using a variety of calibration sources. Based on these comparisons a number of systematic uncertainties were defined to represent possible variations in the event variables relative to the calibrations. In general these included differences in the offset, scale, and resolution for each of the event variables.

We fitted the neutrino signal based on an average $\Phi_{\rm B}$ for day and night, a ν_e survival probability as a function of neutrino energy, E_ν, during the day, $P^{\rm d}_{ee}(E_\nu)$, and an asymmetry between the day and night survival probabilities, $A_{ee}(E_\nu)$, defined by

$$A_{ee}(E_\nu) = 2\frac{P^{\rm n}_{ee}(E_\nu) - P^{\rm d}_{ee}(E_\nu)}{P^{\rm n}_{ee}(E_\nu) + P^{\rm d}_{ee}(E_\nu)}, \tag{1}$$

where $P^{\rm n}_{ee}(E_\nu)$ was the ν_e survival probability during the night. This analysis assumed a constant flux of ^{8}B neutrinos produced by the Sun.

Due to the broad $T_{\rm eff}$ resolution of the detector, $P^{\rm d}_{ee}(E_\nu)$ was not sensitive to sharp distortions and was parameterized by a second order polynomial. Simulations showed that the fit was not sensitive to higher order terms in the polynomial. For the same reasons, $A_{ee}(E_\nu)$ was parameterized by a first order polynomial. By disallowing sharp changes in the neutrino signal that can mimic the background signal at low energies, these parameterizations reduced the covariances between the neutrino interaction and background rates.

4. Results

The total number of neutrons observed in the NCD array equals 1115 ± 79. Figure 1 shows the best fit of the $E_{\rm NCD}$ spectrum. Although the best fit turns down at higher values of $E_{\rm NCD}$, the parameters were consistent with a flat PDF in that region. This variation in the allowed PDF was reflected in the increased statistical uncertainty with higher order polynomials.

The combined fit to all data from SNO yielded a total flux of active neutrino flavors from ^{8}B decays in the Sun of $\Phi_{\rm B}$=$(5.25 \pm 0.16({\rm stat.})^{+0.11}_{-0.13}({\rm syst.})) \times 10^6\,{\rm cm}^{-2}{\rm s}^{-1}$. Figure 2 shows the RMS spread in $P^{\rm d}_{ee}(E_\nu)$ and $A_{ee}(E_\nu)$, taking into account the parameter uncertainties and correlations.

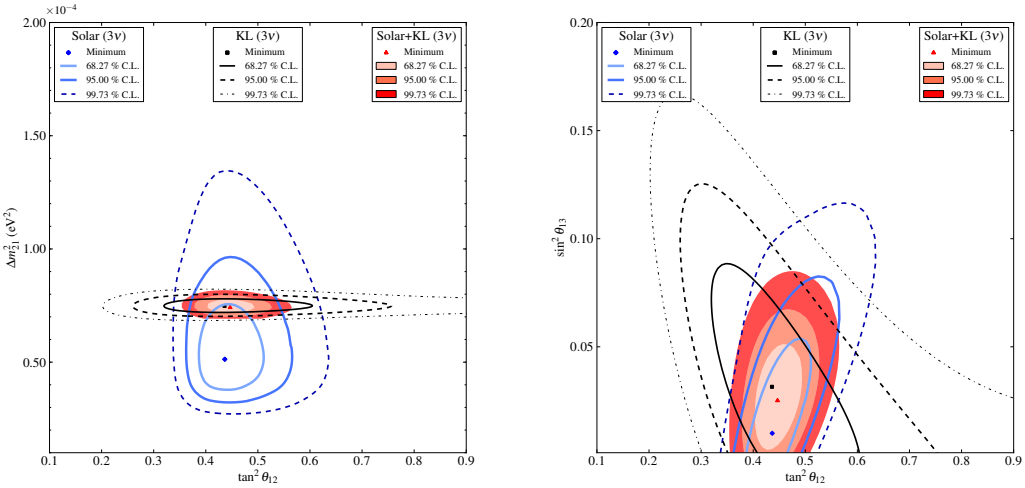

Figure 3. Three-flavor neutrino oscillation analysis contour using both solar neutrino and KamLAND (KL) results.

Figure 3 shows the allowed regions of the $(\tan^2\theta_{12}, \Delta m^2_{21})$ and $(\tan^2\theta_{12}, \sin^2\theta_{13})$ parameter spaces obtained from the results of all solar neutrino experiments[12, 13, 14, 15, 16, 17, 18]. It also shows the result of these experiments combined with the results of the KamLAND experiment, which observed neutrino oscillations in $\bar{\nu}_e$s from nuclear reactors [19]. By assuming CPT invariance we can directly compare these results with the neutrino oscillations observed with solar neutrinos. This results in best fit values of $\tan^2\theta_{12} = 0.446^{+0.030}_{-0.029}$, $\Delta m^2_{21} = (7.41^{+0.21}_{-0.19} \times 10^{-5})\text{eV}^2$, and $\sin^2\theta_{13} = (2.5^{+1.8}_{-1.5}) \times 10^{-2}$ or $\sin^2\theta_{13} < 5.3$ (95% C.L.). Allowing non-zero values of θ_{13} brings the solar neutrino experimental results into better agreement with the results from the KamLAND experiment.

References

[1] Chen H H 1985 *Phys. Rev. Lett.* **55** 1534–1536
[2] Wolfenstein L 1978 *Phys. Rev.* D **17** 2369–2374
[3] Mikheyev S and Smirnov A 1985 *Sov. J. Nucl. Phys.* **42** 913
[4] Maki Z, Nakagawa M and Sakata S 1962 *Prog. Theor. Phys.* **28** 870–880
[5] Pontecorvo B 1958 *Sov. Phys.-JETP* **7** 172–173
[6] Serenelli A M, Basu S, Ferguson J W and Asplund M 2009 *Astrophys. J. Lett.* **705** L123
[7] Aharmim B *et al.* (SNO Collaboration) 2010 *Phys. Rev.* D **81** 055504
[8] Aharmim B *et al.* (SNO Collaboration) 2008 *Phys. Rev. Lett.* **101** 111301
[9] Boger J *et al.* (SNO Collaboration) 2000 *Nucl. Inst. & Meth.* **A449** 172
[10] Amsbaugh J F *et al.* 2007 *Nucl. Inst. & Meth.* **A579** 1054–1080
[11] Aharmim B *et al.* (SNO Collaboration) 2011 Submitted to Phys. Rev. C (*Preprint* `1109.0763`)
[12] Abdurashitov J N *et al.* (SAGE Collaboration) 2009 *Phys. Rev.* C **80** 015807
[13] Cleveland B T *et al.* 1998 *Astrophys. J.* **496** 505–526
[14] Bellini G *et al.* (Borexino Collaboration) 2011 *Phys. Rev. Lett.* **107**(14) 141302
[15] Bellini G *et al.* (Borexino Collaboration) 2010 *Phys. Rev.* D **82** 033006
[16] Hosaka J *et al.* (Super-Kamiokande Collaboration) 2006 *Phys. Rev.* D **73** 112001
[17] Cravens J P *et al.* (Super-Kamiokande Collaboration) 2008 *Phys. Rev.* D **78** 032002
[18] Abe K *et al.* (Super-Kamiokande Collaboration) 2011 *Phys. Rev.* D **83** 052010
[19] Gando A *et al.* (KamLAND Collaboration) 2011 *Phys. Rev.* D **83** 052002